

A consistent equilibrium chemistry algorithm for hypersonic flows*

Frédéric Chalot¹ and Thomas J.R. Hughes²

Division of Applied Mechanics, Durand Building, Stanford University, Stanford, CA 94305-4040, USA

Received 2 December 1992

Revised manuscript received 8 January 1993

The flow past a vehicle traveling at hypersonic speed through the atmosphere is energetic enough to cause vibrational and electronic excitations of the gas particles, as well as trigger chemical reactions. Finite element formulations based on a symmetric form of the conservation laws, such as Galerkin/least-squares, have been developed over the years, and have proved to be successful over a wide range of Mach and Reynolds numbers. They were aimed at solving the Euler and Navier–Stokes equations for perfect gases. Departures from the calorically perfect gas model are considered in the present work, with particular emphasis on thermochemical equilibrium. Applications to re-entry-type flows are presented.

1. Introduction

In extending the Galerkin/least-squares finite element method to hypersonic flows involving chemistry and high-temperature effects, the entropy variables approach may have been expected to engender complications. In fact, not only was no fundamental impediment encountered, but also what seemed to be a consequence of the perfect gas assumption, proves to be quite general.

Although all the material presented subsequently pertains to what we call a general divariant gas, this paper is aimed primarily at the description of equilibrium flows. Before outlining the contents of the paper, we feel it useful to spend some time explaining what we mean by ‘equilibrium flow’ and ‘general divariant gas’. In the thermodynamic sense, equilibrium is defined as the combination of mechanical, thermal and chemical equilibria. Mechanical equilibrium is achieved when there are no unbalanced forces within the considered system or between the system and its surroundings. In the absence of body forces, this leads to uniform velocity and pressure distributions. Thermal equilibrium requires all parts of the system to have the same temperature equal to the temperature of the surroundings. Of course not too many interesting flows have constant pressure, temperature and velocity. However, in many practical instances to the engineer, the assumption of local equilibrium can be made. Under such an assumption, the system can be divided into a collection of microsystems, small on the thermodynamics scale, but large enough to allow certain equilibration processes to take place through particle collisions. Each microsystem is considered in mechanical and thermal equilibrium internally, so that local values of pressure and temperature can be defined. Note that a particular microsystem is not necessarily in equilibrium with the surrounding ones. Molecular processes associated with rotation, vibration and electronic excitation are assumed to be in equilibrium at the translational temperature. This supposes that the corresponding time scales are small compared to that pertinent to the flow field. Obviously this condition cannot be satisfied in regions of the flow where large gradients

Correspondence to: Dr. Thomas J.R. Hughes, CENTRIC Engineering Systems, Inc., 3801 East Bayshore Road, Palo Alto, CA 94303, USA.

* This research was supported by NASA Langley Research Center under Grant NASA-NAG-1-361, and Dassault Aviation, St. Cloud, France.

¹ Also affiliated with Dassault Aviation, 78, quai Marcel Dassault, 92214 St. Cloud, France.

² Also affiliated with CENTRIC Engineering Systems, Inc., 3801 East Bayshore, Palo Alto, CA 94303, USA.

exist, such as behind strong shock waves or in the boundary layer. In addition, small departures from translational equilibrium, such as viscous dissipation and thermal conduction, are taken into account by the Navier–Stokes terms. Hence, in the absence of chemical reactions, the system can be described as a general divariant gas: given an equation of state, its thermodynamic properties are completely defined by any pair of state variables, say pressure and temperature. The equation of state is not limited to that of a thermally perfect gas; in fact, one is not even restricted to the sole description of gases. If the system is chemically reactive, the equilibrium flow assumption requires that the chemical reactions be instantaneous. In other words, each microsystem has a uniform chemical composition which responds instantly to any change in pressure or temperature. Neglecting the chemical kinetics also precludes account of mass diffusion, another translational nonequilibrium phenomenon. However, it still permits the description of the system as a general divariant gas.

A reader unfamiliar with hypersonic flows might wonder why an aerodynamicist would be interested in reacting flows, outside the context of internal flows and combustion. The stagnation temperature in adiabatic flow of a calorifically perfect gas is given by the formula

$$T_0^{\text{PG}} = \left(1 + \frac{\gamma - 1}{2} M_\infty^2\right) T_\infty, \quad (1.1)$$

where M_∞ and T_∞ are, respectively, the free stream Mach number and temperature, and γ is the ratio of specific heats, a constant equal to 1.4 for a calorifically perfect diatomic gas such as air at room temperature. If the distinction between subsonic and supersonic is quite easy, there does not exist such a thing as a ‘hypersonic wall’, marking a clear limit between the supersonic and hypersonic regimes. A good indication might be provided by the breakdown of (1.1) together with the perfect gas assumption, as we will see shortly. In the tables below, we have gathered a few air and space crafts which are milestones in the history of aeronautics and astronautics. Ordered according to increasing Mach numbers, we have: the Wright brothers’ Kitty Hawk Flyer which opened the era of controlled powered flight in 1903; the 747, the first so-called ‘wide-body’ aircraft, introduced by Boeing in 1970; the British/French supersonic transport, the Concorde, whose first experimental flight occurred in 1969; the SR-71 Blackbird, Lockheed’s high-altitude reconnaissance airplane introduced in 1964; the rocket-powered North American X-15, which achieved in 1963 a Mach number of 6.7 at an altitude of 108 km, remaining the second fastest airplane ever built, behind the Space Shuttle; the X-30, a still hypothetical demonstrator for the concept of a hypersonic transport such as the National Aerospace Plane (NASP); the Space Shuttle, built by Rockwell, which became in 1981, after its maiden orbital flight, the first fully reusable vehicle to return from space under aerodynamic control; the Aeroassisted Orbital Transfer Vehicle (AOTV) and its model, the Aeroassist Flight Experiment (AFE), two conceptual designs among others for vehicles that would transfer payloads between earth orbits, depending solely on aerodynamic forces; and last but not least, the Apollo spacecraft, with its historic Mach 36 moon return in 1969. More information about these crafts and the history of flight, can be found in the introduction chapters of [1,2] and in [3]. The Wright brothers obviously encountered no high-temperature hypersonic effects with their top speed of 55 km/h, but the other vehicles merit scrutiny. We have collected in Table 1, the flight conditions and the stagnation temperature as given by (1.1) for each of the crafts. The cruise altitudes and Mach numbers are purely illustrative and, although realistic, are by no means guaranteed to represent the actual performances of the different vehicles. The pressures and temperatures at the different altitudes were taken from the 1966 US Standard Atmosphere [4].

The rise of the temperature in the stagnation region is due to the transfer of the vehicle kinetic energy into the gas particle internal energy (or more rigorously, enthalpy). As can be seen from Table 2, as the Mach number increases, the kinetic energy overshadows the internal energy quite dramatically.

In fact, temperatures do not get as high as predicted according to (1.1). The calorifically perfect gas assumption considers only the translational and rotational modes of molecules to store energy. In the real world, molecules vibrate, have electronic clouds and can take part in chemical reactions. More accurate temperatures computed with the equilibrium chemistry model described in Section 4 are presented in Table 3, together with the relative errors of the ‘perfect gas’ temperatures.

Table 1
Hypersonic flight? What is it?

	M_∞	h (km)	p_∞ (Pa)	T_∞ (K)	T_0^{PG} (K)
Kitty Hawk Flyer	0.046	0	101325	288	288
Boeing 747	0.8	10	26500	223	252
Concorde	2	20	5529	217	391
SR-71	3	30	1197	227	636
X-15	6.7	108	1.068×10^{-2}	227	2265
X-30	15	75	2.516	205	9430
Space Shuttle, NASP	25	75	2.516	205	25830
AOTV, AFE	30	75	2.516	205	37105
Apollo	36	~ 100	3.54×10^{-2}	203	52821

Table 2
Why does the flow get so hot?

	M_∞	T_0^{PG} (K)	e_∞ (kJ/kg)	$ u_\infty ^2/2$ (kJ/kg)
Kitty Hawk Flyer	0.046	288	207.6	0.1
Boeing 747	0.8	252	160.7	28.8
Concorde	2	391	156.4	175.2
SR-71	3	636	163.6	412.2
X-15	6.7	2265	163.6	2056.2
X-30	15	9430	147.8	9307.9
Space Shuttle, NASP	25	25830	147.8	25855.2
AOTV, AFE	30	37105	147.8	37231.5
Apollo	36	52821	146.3	53092.8

Table 3
In fact, it does not get that hot!

	M_∞	T_0^{PG} (K)	T_0^{equil} (K)	Error (%)
Kitty Hawk Flyer	0.046	288	288	0.0
Boeing 747	0.8	252	252	0.0
Concorde	2	391	390	0.3
SR-71	3	636	628	1.3
X-15	6.7	2265	1818	24.6
X-30	15	9430	4210	124.0
Space Shuttle, NASP	25	25830	5812	463.1
AOTV, AFE	30	37105	6850	441.7
Apollo	36	52821	~ 11000	380.2

From Table 3, it appears clear that major departures from the perfect gas model occur only above Mach 5, which is the value generally agreed upon for the limit of hypersonic flight in air. Atmospheres with different gas composition, pressure and temperature distribution, could see this value either increase or decrease.

An outline of the paper follows. In the next section, we derive the symmetric form of the Euler and Navier–Stokes equations for a general divariant gas. In Section 3, we describe briefly the Galerkin/least-squares finite element formulation. In Section 4, we propose a simple equilibrium chemistry model for air. In Section 5, before giving some concluding remarks, we present a few numerical examples which confirm the practical computer implementation of the method.

2. Symmetric Euler and Navier–Stokes equations for a general divariant gas

As a starting point, we consider the Euler and Navier–Stokes equations written in conservative form:

$$U_{,t} + F_{i,i}^{\text{adv}} = F_{i,i}^{\text{diff}}, \quad (2.1)$$

where \mathbf{U} is the vector of conservative variables; $\mathbf{F}_i^{\text{adv}}$ and $\mathbf{F}_i^{\text{diff}}$ are, respectively, the advective and the diffusive fluxes in the i th-direction. Inferior commas denote partial differentiation and repeated indices indicate summation. In three dimensions, \mathbf{U} , $\mathbf{F}_i^{\text{adv}}$, and $\mathbf{F}_i^{\text{diff}}$ read

$$\mathbf{U} = \rho \begin{Bmatrix} 1 \\ \mathbf{u} \\ e^{\text{tot}} \end{Bmatrix}, \quad (2.2)$$

$$\mathbf{F}_i^{\text{adv}} = u_i \mathbf{U} + p \begin{Bmatrix} 0 \\ \boldsymbol{\delta}_i \\ u_i \end{Bmatrix}, \quad \mathbf{F}_i^{\text{diff}} = \mathbf{F}_i^{\text{visc}} + \mathbf{F}_i^{\text{heat}}, \quad (2.3)$$

$$\mathbf{F}_i^{\text{visc}} = \begin{Bmatrix} 0 \\ \tau_{ij} \boldsymbol{\delta}_j \\ \tau_{ij} u_j \end{Bmatrix}, \quad \mathbf{F}_i^{\text{heat}} = \begin{Bmatrix} 0 \\ \mathbf{0}_3 \\ -q_i \end{Bmatrix}, \quad (2.4)$$

where ρ is the density; $\mathbf{u} = \{u_1, u_2, u_3\}^t$ is the velocity vector; e^{tot} is the total energy per unit mass, which is the sum of the internal energy per unit mass, e , and of the kinetic energy per unit mass, $|\mathbf{u}|^2/2$; p is the thermodynamic pressure; and $\boldsymbol{\delta}_i = \{\delta_{ij}\}$ is a generalized Kronecker delta vector, where δ_{ij} is the usual Kronecker delta (viz., $\delta_{ii} = 1$, and $\delta_{ij} = 0$ for $i \neq j$). The diffusive flux, which constitutes a first order correction taking into account translational nonequilibrium effects, splits up into two parts: a viscous stress part, $\mathbf{F}_i^{\text{visc}}$, and a heat conduction part, $\mathbf{F}_i^{\text{heat}}$. Furthermore, $\boldsymbol{\tau} = [\tau_{ij}]$ is the viscous-stress tensor; $\mathbf{q} = \{q_1, q_2, q_3\}^t$ is the heat-flux vector; and $\mathbf{0}_3$ is the null vector of length three.

The definition of the diffusive flux is completed by the following constitutive relations:

(i) The viscous stress tensor $\boldsymbol{\tau}$ is given by

$$\tau_{ij} = \lambda^{\text{visc}} u_{k,k} \delta_{ij} + \mu^{\text{visc}} (u_{i,j} + u_{j,i}), \quad (2.5)$$

where λ^{visc} and μ^{visc} are the viscosity coefficients. λ^{visc} may be defined in terms of μ^{visc} and the bulk viscosity coefficient μ_B^{visc} by

$$\lambda^{\text{visc}} = \mu_B^{\text{visc}} - \frac{2}{3} \mu^{\text{visc}}. \quad (2.6)$$

For perfect monatomic gases, kinetic theory predicts that $\mu_B^{\text{visc}} = 0$. Stokes' hypothesis states that μ_B^{visc} can be taken equal to zero in the general case. However, as shown by Vincenti and Kruger [5], behaviors such as small departures from rotational equilibrium can be represented by means of bulk viscosity. In the present discussion, where thermal equilibrium is assumed, Stokes' hypothesis is valid.

(ii) The heat flux is given by the usual Fourier law,

$$q_i = -\kappa T_{,i}, \quad (2.7)$$

where κ is the coefficient of thermal conductivity.

Equation (2.1) can be rewritten in so-called quasi-linear form:

$$U_{,i} + \mathbf{A}_i U_{,i} = (\mathbf{K}_{ij} U_{,j})_{,i}, \quad (2.8)$$

where $\mathbf{A}_i = \mathbf{F}_{i,U}^{\text{adv}}$ is the i th advective Jacobian matrix, and $\mathbf{K} = [\mathbf{K}_{ij}]$ is the diffusivity matrix, defined by $\mathbf{F}_i^{\text{diff}} = \mathbf{K}_{ij} U_{,j}$. The \mathbf{A}_i 's and \mathbf{K} do not possess any particular property of symmetry or positiveness.

We now introduce a new set of variables,

$$\mathbf{V}^t = \frac{\partial \mathcal{H}}{\partial \mathbf{U}}, \quad (2.9)$$

where \mathcal{H} is the generalized entropy function given by

$$\mathcal{H} = \mathcal{H}(U) = -\rho s \quad (2.10)$$

and s is the thermodynamic entropy per unit mass. Under the change of variables $U \mapsto V$, (2.8) becomes

$$\tilde{A}_0 V_{,t} + \tilde{A}_i V_{,i} = (\tilde{K}_{ij} V_{,j})_{,i}, \quad (2.11)$$

where

$$\tilde{A}_0 = U_{,V}, \quad (2.12)$$

$$\tilde{A}_i = A_i \tilde{A}_0, \quad (2.13)$$

$$\tilde{K}_{ij} = K_{ij} \tilde{A}_0. \quad (2.14)$$

The Riemannian metric tensor \tilde{A}_0 is symmetric positive-definite; the \tilde{A}_i 's are symmetric; and $\tilde{K} = [\tilde{K}_{ij}]$ is symmetric positive-semidefinite. In view of these properties, (2.11) is referred to as a symmetric advective-diffusive system.

For a general divariant gas, the vector of so-called (physical) entropy variables, V , reads

$$V = \frac{1}{T} \begin{Bmatrix} \mu - |u|^2/2 \\ u \\ -1 \end{Bmatrix}, \quad (2.15)$$

where $\mu = e + pv - Ts$ is the chemical potential per unit mass; $v = 1/\rho$ is the specific volume. In order to derive (2.15), we used Gibbs' equation written for a divariant gas (s is a function of e and v only):

$$ds = \frac{1}{T} (de + p dv). \quad (2.16)$$

The Riemannian metric tensor \tilde{A}_0 and the advective Jacobian matrices \tilde{A}_i require an additional equation of state to complete their definitions. For that purpose, we assume given a relation which provides the chemical potential of the gas in terms of its thermodynamical state, e.g.,

$$\mu = \mu(p, T). \quad (2.17)$$

All thermodynamic quantities relevant to the formation of (2.11) can then be computed:

$$s = -\left(\frac{\partial \mu}{\partial T}\right)_p, \quad v = \left(\frac{\partial \mu}{\partial p}\right)_T, \quad (2.18)$$

$$h = \mu + Ts, \quad e = h - pv, \quad (2.19)$$

$$\alpha_p = \frac{1}{v} \left(\frac{\partial v}{\partial T}\right)_p = \frac{1}{v} \left(\frac{\partial^2 \mu}{\partial p \partial T}\right), \quad \beta_T = -\frac{1}{v} \left(\frac{\partial v}{\partial p}\right)_T = -\frac{1}{v} \left(\frac{\partial^2 \mu}{\partial p^2}\right)_T, \quad (2.20)$$

$$c_p = \left(\frac{\partial h}{\partial T}\right)_p = -T \left(\frac{\partial^2 \mu}{\partial T^2}\right)_p, \quad c_v = \left(\frac{\partial e}{\partial T}\right)_v = c_p - \frac{\alpha_p^2 v T}{\beta_T}. \quad (2.21)$$

where α_p is the coefficient of volume expansion, β_T is the isothermal compressibility, and c_p and c_v are the specific heats at constant pressure and volume. As an example, the Riemannian metric tensor \tilde{A}_0 reads

$$\tilde{\mathbf{A}}_0 = \frac{\beta_T T}{v^2} \begin{bmatrix} 1 & u_1 & u_2 & u_3 & h + \frac{|\mathbf{u}|^2}{2} - \frac{v\alpha_p T}{\beta_T} \\ u_1^2 + \frac{v}{\beta_T} & u_1 u_2 & u_1 u_3 & u_1 \left(h + \frac{|\mathbf{u}|^2}{2} - \frac{v(\alpha_p T - 1)}{\beta_T} \right) \\ & u_2^2 + \frac{v}{\beta_T} & u_2 u_3 & u_2 \left(h + \frac{|\mathbf{u}|^2}{2} - \frac{v(\alpha_p T - 1)}{\beta_T} \right) \\ \text{symm.} & & u_3^2 + \frac{v}{\beta_T} & u_3 \left(h + \frac{|\mathbf{u}|^2}{2} - \frac{v(\alpha_p T - 1)}{\beta_T} \right) \\ & & & a_{55} \end{bmatrix}, \quad (2.22)$$

where

$$a_{55} = (h + \frac{1}{2}|\mathbf{u}|^2)^2 + \frac{v}{\beta_T}(c_p T - 2h\alpha_p T - |\mathbf{u}|^2(\alpha_p T - 1)). \quad (2.23)$$

All other coefficient matrices can be found in [6].

Taking the dot product of (2.11) with the vector \mathbf{V} yields the Clausius–Duhem inequality, which constitutes the basic nonlinear stability condition for the solutions of (2.11). This fundamental property is inherited by appropriately defined finite element methods, such as that described in the next section.

3. The Galerkin/least-squares formulation

The Galerkin/least-squares formulation introduced by Hughes [7–9] and Johnson [10, 11], is a full space-time finite element technique employing the discontinuous Galerkin method in time (see [12]). The least-squares operator improves the stability of the method while retaining accuracy. A nonlinear discontinuity-capturing operator is added in order to enhance the local behavior of the solution in the vicinity of sharp gradients.

We consider the time interval $I =]0, T[$, which we subdivide into N intervals $I_n =]t_n, t_{n+1}[$, $n = 0, \dots, N-1$. Let

$$Q_n = \Omega \times I_n \quad (3.1)$$

and

$$P_n = \Gamma \times I_n, \quad (3.2)$$

where Ω is the spatial domain of interest, and Γ is its boundary. In turn, the space-time ‘slab’ Q_n is tiled by $(n_{\text{el}})_n$ elements Q_n^e . Consequently, the Galerkin/least-squares variational problem can be stated as: Within each Q_n , $n = 0, \dots, N-1$, find $\mathbf{V}^h \in \mathcal{V}_n^h$ (trial function space), such that for all $\mathbf{W}^h \in \mathcal{V}_n^h$ (weighting function space), the following equation holds:

$$\begin{aligned} & \int_{Q_n} (-\mathbf{W}_{,i}^h \cdot \mathbf{U}(\mathbf{V}^h) - \mathbf{W}_{,i}^h \cdot \mathbf{F}_i^{\text{adv}}(\mathbf{V}^h) + \mathbf{W}_{,i}^h \cdot \tilde{\mathbf{K}}_{ij} \mathbf{V}_{,j}^h) \, dQ \\ & + \int_{\Omega} (\mathbf{W}^h(t_{n+1}^-) \cdot \mathbf{U}(\mathbf{V}^h(t_{n+1}^-)) - \mathbf{W}^h(t_n^+) \cdot \mathbf{U}(\mathbf{V}^h(t_n^+))) \, d\Omega \\ & + \sum_{e=1}^{(n_{\text{el}})_n} \int_{Q_n^e} (\mathcal{L}\mathbf{W}^h) \cdot \boldsymbol{\tau}(\mathcal{L}\mathbf{V}^h) \, dQ \\ & + \sum_{e=1}^{(n_{\text{el}})_n} \int_{Q_n^e} v^h g^{ij} \mathbf{W}_{,i}^h \cdot \tilde{\mathbf{A}}_0 \mathbf{V}_{,j}^h \, dQ \\ & = \int_{P_n} \mathbf{W}^h \cdot (-\mathbf{F}_i^{\text{adv}}(\mathbf{V}^h) + \mathbf{F}_i^{\text{diff}}(\mathbf{V}^h)) n_i \, dP. \end{aligned} \quad (3.3)$$

The first and last integrals represent the Galerkin formulation written in integrated-by-parts form. The solution space consists of piecewise polynomials which are continuous in space, but are discontinuous across time slabs. Continuity in time is weakly enforced by the second integral in (3.3), which contributes to the jump condition between two contiguous slabs, with

$$\mathbf{Z}^h(t_n^\pm) = \lim_{\epsilon \rightarrow 0^\pm} \mathbf{Z}^h(t_n + \epsilon). \quad (3.4)$$

The third integral constitutes the least-squares operator where \mathcal{L} is defined as

$$\mathcal{L} = \tilde{\mathbf{A}}_0 \frac{\partial}{\partial t} + \tilde{\mathbf{A}}_i \frac{\partial}{\partial x_i} - \frac{\partial}{\partial x_i} \left(\tilde{\mathbf{K}}_{ij} \frac{\partial}{\partial x_j} \right). \quad (3.5)$$

τ is a symmetric matrix for which definitions can be found in [13, 14]. The fourth integral is the nonlinear discontinuity-capturing operator, which is designed to control oscillations about discontinuities, without upsetting higher-order accuracy in smooth regions. g^{ij} is the contravariant metric tensor defined by

$$[g^{ij}] = [\xi_{,i} \cdot \xi_{,j}]^{-1}, \quad (3.6)$$

where $\xi = \xi(\mathbf{x})$ is the inverse isoparametric element mapping, and ν^h is scalar-valued homogeneous function of the residual $\mathcal{L}\mathbf{V}^h$. The discontinuity capturing factor ν^h used in the present work is an extension of that introduced in [14–16].

A key ingredient to the formulation is its consistency: the exact solution of (2.1) satisfies the variational formulation (3.3). This constitutes an essential property in order to attain higher-order spatial convergence. In addition, it must be noted that the numerical method presented here does not rely on the advective fluxes being homogeneous in the conservative variables, which is true only for a thermally perfect gas (see [6]). More complex equations of state such as those needed for describing equilibrium chemistry, do not require any particular approximation to be introduced, which is often the case with other techniques. One can say that the formulation is consistent with the equation of state. For further details about the method, the reader is referred to the works mentioned in this section.

4. A simple chemistry model for equilibrium air

In this section, we describe a chemistry model for equilibrium air. Although it is simple, it encompasses all the ingredients necessary to compute the composition of the gas mixture and the quantities (2.18)–(2.21). The state of the system is given by the vector of entropy variables, from which the chemical potential of the mixture μ and its temperature T can be extracted trivially. On the other hand, a solver based on conservative variables would typically have the density ρ and the internal energy e at its disposal to define the thermodynamic state of the system. We find the entropy variables advantageous here, since temperature is a more convenient variable than density, especially to express quantities such as energies (internal energy, Gibbs' free energy, etc.).

We consider air as a mixture of five thermally perfect gases: N_2 , O_2 , NO , N and O . Given the thermodynamic state of the system (μ, T) , we propose to compute the equilibrium partial pressure of each component, and the quantities (2.18)–(2.21). In order to solve for the five p_s 's, we need five independent equations.

First, we can write the chemical potential μ as a function of the p_s 's and T :

$$\sum_s y_s(\mathbf{p}) \mu_s(p_s, T) = \mu, \quad (4.1)$$

where y_s and μ_s are respectively the mass fraction and the chemical potential of species s , and $\mathbf{p} = \{p_s\}$

is the vector of partial pressures. The mass fraction y_s is related to the mole fraction x_s and the molar mass \hat{M}_s of species s , and to the molar mass \hat{M} of the mixture by

$$y_s = \frac{\hat{M}_s}{\hat{M}} x_s . \quad (4.2)$$

In turn, x_s and \hat{M} are given in terms of the partial pressures by

$$x_s = \frac{p_s}{p} \quad (4.3)$$

and

$$\hat{M} = \sum_s x_s \hat{M}_s . \quad (4.4)$$

The pressure is provided by Dalton's law of partial pressures:

$$p = \sum_s p_s . \quad (4.5)$$

Each species being considered as a thermally perfect gas, we have

$$p_s = \rho_s R_s T , \quad (4.6)$$

where ρ_s and R_s are respectively the density and the specific gas constant of species s . R_s is linked to the universal gas constant $\hat{R} = 8.31441 \text{ J/mol K}$ through

$$R_s = \frac{\hat{R}}{\hat{M}_s} . \quad (4.7)$$

The chemical potential of species s is

$$\mu_s = h_s - Ts_s , \quad (4.8)$$

where, in the thermally perfect gas case,

$$h_s = e_s(T) + R_s T , \quad (4.9)$$

$$s_s = \int \frac{de_s}{T} + R_s \ln T - R_s \ln p_s + s_{0s} . \quad (4.10)$$

The internal energy e_s is a function of temperature only, and s_{0s} is the specific reference entropy upon which we will elaborate later. We adopt the rigid-rotator and harmonic-oscillator model. Under this assumption, a simple closed form expression exists for the internal energy. It splits up into a translational, a rotational and a vibrational contribution, to which the heat of formation h_s^0 must be added:

$$e_s(T) = e_s^{\text{trans}} + e_s^{\text{rot}} + e_s^{\text{vib}} + h_s^0 \quad (4.11)$$

$$e_s^{\text{trans}}(T) = 3 \times \frac{1}{2} R_s T , \quad (4.12)$$

$$e_s^{\text{rot}}(T) = \begin{cases} 0 , & \text{for atoms ,} \\ 2 \times \frac{1}{2} R_s T , & \text{for diatomic molecules ,} \end{cases} \quad (4.13)$$

$$e_s^{\text{vib}}(T) = \begin{cases} 0, & \text{for atoms,} \\ \frac{R_s \Theta_s^{\text{vib}}}{\exp(\Theta_s^{\text{vib}}/T) - 1}, & \text{for diatomic molecules.} \end{cases} \quad (4.14)$$

We ignore any electronic contribution to the internal energy. This makes the model simpler, but does not limit the generality of the present development. Equation (4.10) can now be integrated exactly, yielding

$$s_s = \frac{e_s^{\text{vib}}}{T} - R_s \ln[1 - \exp(-\Theta_s^{\text{vib}}/T)] + c_{ps} \ln T - R_s \ln p_s + s_{0s}, \quad (4.15)$$

where

$$c_{ps} = c_{vs} + R_s = \begin{cases} \frac{5}{2} R_s, & \text{for atoms,} \\ \frac{7}{2} R_s, & \text{for diatomic molecules.} \end{cases} \quad (4.16)$$

Finally, μ_s is given by

$$\mu_s = c_{ps} T(1 - \ln T) + R_s T \ln p_s + h_s^0 + R_s T \ln[1 - \exp(-\Theta_s^{\text{vib}}/T)] - T s_{0s}. \quad (4.17)$$

We introduce the molar chemical potentials

$$\begin{aligned} \hat{\mu}_s &= \hat{M}_s \mu_s = \hat{c}_{ps} T(1 - \ln T) + \hat{R} T \ln p_s + \hat{h}_s^0 + \hat{R} T \ln[1 - \exp(-\Theta_s^{\text{vib}}/T)] - T \hat{s}_{0s} \\ &= \hat{\mu}_s^0(T) + \hat{R} T \ln p_s \end{aligned} \quad (4.18)$$

where $\hat{\mu}_s^0$ is the molar chemical potential of species s in the pure state and at unit pressure. Equation (4.1) can be restated as

$$\sum_s p_s (\hat{\mu}_s - \hat{M}_s \mu) = 0. \quad (4.19)$$

This constitutes the first equation of our system.

The second equation is obtained by stating that the local proportion of nitrogen atoms relative to oxygen atoms is constant, viz.,

$$\frac{2x_{\text{N}_2} + x_{\text{NO}} + x_{\text{N}}}{2x_{\text{O}_2} + x_{\text{NO}} + x_{\text{O}}} = \frac{79}{21}, \quad (4.20)$$

where we have assumed that air is a mixture of 79% of nitrogen and 21% of oxygen by volume. In terms of partial pressures, (4.20) can be rewritten as

$$\frac{2p_{\text{N}_2} + p_{\text{NO}} + p_{\text{N}}}{2p_{\text{O}_2} + p_{\text{NO}} + p_{\text{O}}} = \frac{79}{21}. \quad (4.21)$$

In addition to (4.19) and (4.21), we need three more equations. These are provided by three independent chemical reactions,



We can write the law of mass action for each of these. For consistency, we do not state the equilibrium condition for reaction R is the usual form, i.e.,

$$\prod_s p_s^{\nu_{sR}} = K_{pR}(T), \quad (4.25)$$

where ν_{sR} is the stoichiometric coefficient of species s in reaction R , and $K_{pR}(T)$ the equilibrium constant of reaction R . The latter is a function of temperature which is often given in the form of a curve fit of experimental results. In place of (4.25), we write for each reaction the following statement which is equivalent, but does not require any extraneous data:

$$\sum_s \nu_{sR} \hat{\mu}_s = 0. \quad (4.26)$$

Once a model has been chosen for the internal energies of the different species, the system is closed, and the addition of any superfluous piece of information, such as equilibrium constants, can only introduce inconsistencies. However, in order to use the chemical potentials given by (4.18) in the equation for reaction equilibrium (4.26), the absolute entropy must be computed carefully, and in particular the integration constant \hat{s}_{0s} . It is provided by statistical mechanics, and is the sum of four terms,

$$\hat{s}_{0s} = \hat{s}_{0s}^{\text{trans}} + \hat{s}_{0s}^{\text{rot}} + \hat{s}_{0s}^{\text{vib}} + \hat{s}_{0s}^{\text{el}}, \quad (4.27)$$

where

$$\hat{s}_{0s}^{\text{trans}} = \hat{R} \left\{ \ln \left[\left(\frac{2\pi m_s}{h^2} \right)^{3/2} k^{5/2} \right] + \frac{5}{2} \right\}, \quad (4.28)$$

$$\hat{s}_{0s}^{\text{rot}} = \hat{R} (1 - \ln \sigma_s \Theta_s^{\text{rot}}), \quad (4.29)$$

$$\hat{s}_{0s}^{\text{vib}} = 0, \quad (4.30)$$

$$\hat{s}_{0s}^{\text{el}} = \hat{R} \ln g_{0s}. \quad (4.31)$$

Equation (4.28) is known as the Sackur–Tetrode formula, in which m_s is the mass of one particle of species s :

$$m_s = \frac{\hat{M}_s}{\hat{N}}; \quad (4.32)$$

$\hat{N} = 6.022045 \times 10^{23}$ is Avogadro's number; $h = 6.626176 \times 10^{-34}$ J s is Planck's constant; and Boltzmann's constant k is given by

$$k = \frac{\hat{R}}{\hat{N}}. \quad (4.33)$$

Table 4
Chemical model constants

	N ₂	O ₂	NO	N	O
\hat{M}_s (kg/mol)	28×10^{-3}	32×10^{-3}	30×10^{-3}	14×10^{-3}	16×10^{-3}
\hat{h}_s^0 (J/mol)	0	0	89775	470820	246790
Θ_s^{vib} (K)	3393.50	2273.56	2738.87	—	—
Θ_s^{rot} (K)	2.87	2.08	2.45	—	—
σ_s	2	2	1	—	—
g_{0s}	1	3	4	4	9

In the rotational part $\hat{s}_{0s}^{\text{rot}}$, σ_s is the symmetry factor of the molecule and Θ_s^{rot} is its characteristic temperature for rotation. Although we have neglected any electronic excitation, we must take into account the degeneracy of the ground level, which yields zero energy, but is crucial for a correct evaluation of the reference entropy. The constants used in the present model are gathered in Table 4. For the most part, they were taken from [17].

Finally, for the three independent chemical reactions (4.22)–(4.24), (4.33) reads

$$\hat{\mu}_{\text{N}_2} = 2\hat{\mu}_{\text{N}}, \quad (4.34)$$

$$\hat{\mu}_{\text{O}_2} = 2\hat{\mu}_{\text{O}}, \quad (4.35)$$

$$\hat{\mu}_{\text{NO}} = \hat{\mu}_{\text{N}} + \hat{\mu}_{\text{O}}. \quad (4.36)$$

The resulting system of five nonlinear equations for the p_s 's in terms of μ and T ((4.19), (4.21), (4.34)–(4.36)) can formally be expressed as

$$f(\mathbf{p}, \mu, T) = \mathbf{0}, \quad (4.37)$$

where

$$f = \begin{Bmatrix} \sum_s p_s (\hat{\mu}_s - \hat{M}_s \mu) \\ 42p_{\text{N}_2} - 158p_{\text{O}_2} - 58p_{\text{NO}} + 21p_{\text{N}} - 79p_{\text{O}} \\ 2\hat{\mu}_{\text{N}} - \hat{\mu}_{\text{N}_2} \\ 2\hat{\mu}_{\text{O}} - \hat{\mu}_{\text{O}_2} \\ \hat{\mu}_{\text{N}} + \hat{\mu}_{\text{O}} - \hat{\mu}_{\text{NO}} \end{Bmatrix}. \quad (4.38)$$

The system (4.37) is solved using the Newton–Raphson method: given an initial guess $\mathbf{p}^{(0)}$ for \mathbf{p} , the $(n+1)$ st iterate is defined by

$$\mathbf{p}^{(n+1)} = \mathbf{p}^{(n)} + \Delta \mathbf{p}^{(n)}, \quad (4.39)$$

where

$$\Delta \mathbf{p}^{(n)} = -J^{-1}(\mathbf{p}^{(n)}, \mu, T) f(\mathbf{p}^{(n)}, \mu, T) \quad (4.40)$$

and

$$J = \left(\frac{\partial f}{\partial \mathbf{p}} \right)_{\mu, T}. \quad (4.41)$$

A good initial guess assures quadratic convergence of the process. Typically, the p_s 's are computed up to ten significant digits in two iterations. Initial values for the partial pressures are obtained from a table look-up.

Once convergence of the Newton scheme has been achieved, the Jacobian J satisfies

$$J d\mathbf{p} + \left(\frac{\partial f}{\partial \mu} \right)_{\mathbf{p}, T} d\mu + \left(\frac{\partial f}{\partial T} \right)_{\mathbf{p}, \mu} dT = \mathbf{0}, \quad (4.42)$$

which is the differential of (4.37). Thus,

$$d\mathbf{p} = -J^{-1} \left(\frac{\partial f}{\partial \mu} \right)_{\mathbf{p}, T} d\mu - J^{-1} \left(\frac{\partial f}{\partial T} \right)_{\mathbf{p}, \mu} dT \quad (4.43)$$

and

$$\left(\frac{\partial \mathbf{p}}{\partial \mu} \right)_T = -J^{-1} \left(\frac{\partial f}{\partial \mu} \right)_{\mathbf{p}, T} \quad (4.44)$$

$$\left(\frac{\partial \mathbf{p}}{\partial T}\right)_\mu = -\mathbf{J}^{-1} \left(\frac{\partial \mathbf{f}}{\partial T}\right)_{p,\mu}. \quad (4.45)$$

These derivatives are obtained at essentially no extra cost, since in practice we use the LU -decomposition of the last iteration Jacobian. From (4.44) and (4.45), we can calculate any thermodynamic derivative. For instance, the partial derivatives of the mass fractions with respect to pressure and temperature are given by

$$\left(\frac{\partial y_s}{\partial p}\right)_T = y_s \left[\frac{1}{p_s} \left(\frac{\partial p_s}{\partial p}\right)_T - \sum_r \frac{y_r}{p_r} \left(\frac{\partial p_r}{\partial p}\right)_T \right], \quad (4.46)$$

$$\left(\frac{\partial y_s}{\partial T}\right)_p = y_s \left[\frac{1}{p_s} \left(\frac{\partial p_s}{\partial T}\right)_p - \sum_r \frac{y_r}{p_r} \left(\frac{\partial p_r}{\partial T}\right)_p \right], \quad (4.47)$$

where

$$\left(\frac{\partial p_s}{\partial p}\right)_T = \frac{\left(\frac{\partial p_s}{\partial \mu}\right)_T}{\sum_r \left(\frac{\partial p_r}{\partial \mu}\right)_T}, \quad (4.48)$$

$$\left(\frac{\partial p_s}{\partial T}\right)_p = \left(\frac{\partial p_s}{\partial T}\right)_\mu - \frac{\sum_r \left(\frac{\partial p_r}{\partial T}\right)_\mu}{\sum_r \left(\frac{\partial p_r}{\partial \mu}\right)_T} \left(\frac{\partial p_s}{\partial \mu}\right)_T. \quad (4.49)$$

We now have everything at our disposal to compute the quantities required to form (2.11). For instance, we have

$$c_p = \left(\frac{\partial h}{\partial T}\right)_p = \sum_s y_s \left(\frac{\partial h_s}{\partial T}\right)_p + \sum_s \left(\frac{\partial y_s}{\partial T}\right)_p h_s, \quad (4.50)$$

$$\alpha_p = \frac{1}{v} \left(\frac{\partial v}{\partial T}\right)_p = \frac{1}{T} + \frac{1}{R} \sum_s \left(\frac{\partial y_s}{\partial T}\right)_p R_s, \quad (4.51)$$

$$\beta_T = -\frac{1}{v} \left(\frac{\partial v}{\partial p}\right)_T = \frac{1}{p} - \frac{1}{R} \sum_s \left(\frac{\partial y_s}{\partial p}\right)_T R_s, \quad (4.52)$$

$$c_v = c_p - \frac{\alpha_p^2 v T}{\beta_T}, \quad (4.53)$$

$$a^2 = \frac{v c_p}{c_v \beta_T}, \quad (4.54)$$

where a is the speed of sound.

The techniques portrayed in this section may seem elaborate for a simple chemistry model. In fact, all the ingredients necessary for dealing with the most complex situation are contained within the previous description.

5. Numerical examples

We now present two sets of two-dimensional computations which illustrate the procedures described in the preceding sections. The first contrasts the perfect gas and the equilibrium chemistry solutions for

the same inviscid case; the second compares viscous and inviscid treatments of the flow past a space-shuttle like configuration.

The spatial domains are meshed using unstructured combinations of bilinear quadrilaterals and linear triangles. Adaptive refinement is introduced in both the shock and the boundary layer regions; we will elaborate on this strategy when we describe the individual test cases and especially the Navier–Stokes case.

Convergence to steady state is achieved with the help of a first-order-in-time low-storage fully implicit iterative solver based on the preconditioned GMRES algorithm (see [14, 18, 19]).

5.1. Flow over a blunt body

The geometry is a simple circular cylinder of unit radius extended with two planes at 15° angle. The body faces an inviscid Mach 17.9 flow at zero angle of attack. The free stream density and temperature are respectively 10^{-4} kg/m^3 and 231 K. This test case is described by Désidéri et al. in [20]. Figure 1 compares the equilibrium chemistry solution (top) with the perfect gas one (bottom) for the same inflow conditions. In view of the symmetry of the problem, the computation is performed on half the domain only. The ‘chemistry’ mesh contains 4378 nodes and 8573 elements; the ‘perfect gas’ one 4856 nodes and 9527 elements. Both meshes consist of triangular elements, and are adaptively enriched in order to better capture the detached bow shock. Figure 1 presents both meshes (a), pressure (b) and temperature (c) contours. The difference between the two equations of state appears quite clearly: the stand-off distance of the shock is much reduced in the more realistic equilibrium chemistry case. In addition, the temperature rise through the shock goes down by a factor of almost 3. The numerical results are found in remarkable agreement with the theoretical solutions. Typically, the relative error on all stagnation values is under 0.5%, with minima still an order of magnitude below this value (e.g., the stagnation temperature in the equilibrium case is overestimated by a mere 0.0582%). In an industrial setting, the additional cost due to the chemistry routine might be a real concern. In fact, it turns out that the cost of an equilibrium chemistry computation is only about 20% higher than that of a perfect gas computation. Specially designed curve fits may further reduce this figure.

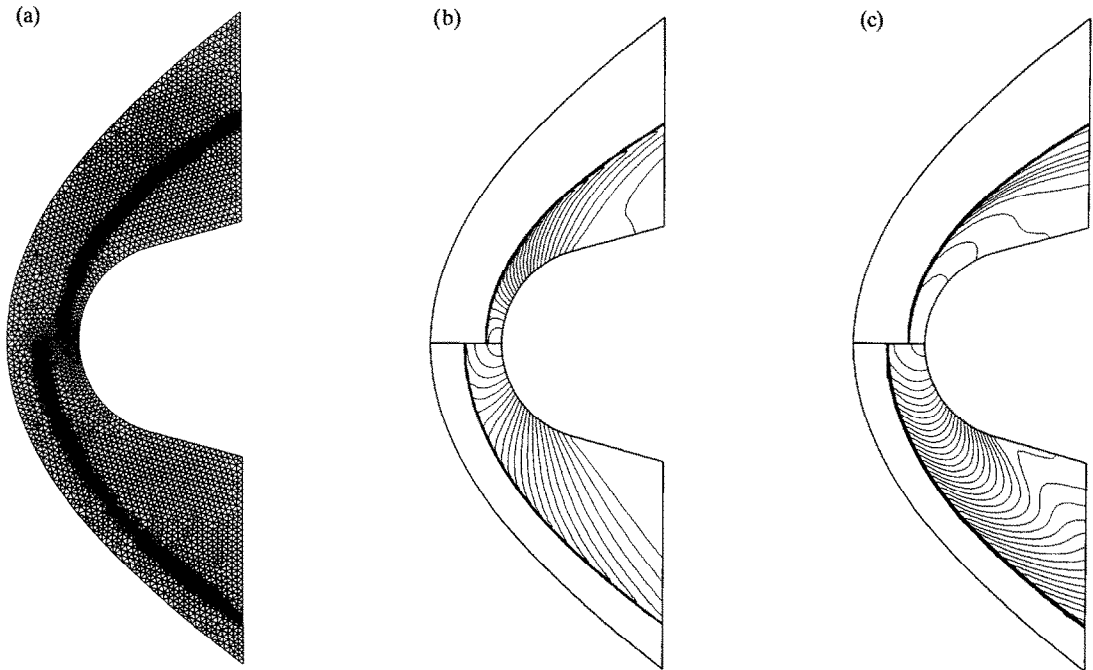


Fig. 1. Flow past a blunt body. Top: equilibrium chemistry; bottom: perfect gas. (a) Mesh; (b) pressure contours; (c) temperature contours.

5.2. Flow over a double ellipse

With this example, we compare the Euler and the Navier–Stokes solutions of the same flow over a generic space-shuttle geometry given by a double ellipse. The inflow Mach number is 25; the angle of attack is 30° . The free stream conditions simulate a 75 km altitude in the US Standard Atmosphere [4]: $T_\infty = 205.3$ K and $p_\infty = 2.52$ Pa. For the viscous case, the Reynolds number is 22 000/m; the geometry measures 0.76 m in length, with the major half axis of the larger ellipse being 0.6 m long; the wall temperature is fixed at 1500 K. These test cases are two-dimensional variants of cases proposed at the Workshop on Hypersonic Flows for Re-entry Problems—Part II, held in Antibes, France, 15–19 April 1991.

The meshes employed are shown in Figs. 2 and 3. The Euler mesh consists of 8307 nodes and 16 231 triangular elements. The Navier–Stokes mesh which contains 10 613 nodes, is an unstructured combination of 13 605 triangles in the main flow and of 3620 quadrilaterals along the body. The structured strip is made of 20 layers of quadrilateral elements; its thickness is adapted to match that of the boundary layer. This strategy, while maintaining the advantages of unstructuredness, facilitates capturing the fine features of the boundary layer. In addition, both meshes are enriched in the shock region. Figures 4–11 present the pressure, temperature, N and O mass fraction contours for the inviscid (left) and the viscous (right) cases. As one would expect, the pressure contours are quite similar for the two solutions. The Navier–Stokes solution shows, however, a clear recombination of nitrogen and oxygen at the wall. The canopy shock present in the Euler solution has nearly completely vanished in the viscous calculation. Finally, one must note the extreme thinness of the boundary layer on the windward side of the body.

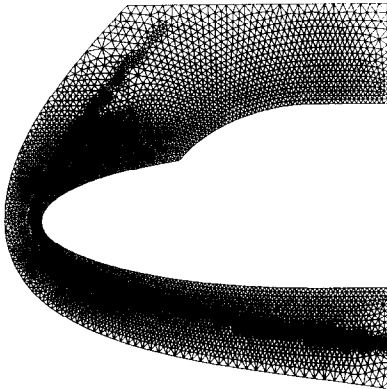


Fig. 2. Mesh: 8307 nodes, 16 231 elements (inviscid case).

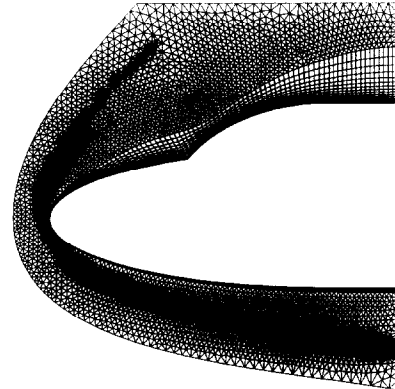


Fig. 3. Mesh: 10 613 nodes, 17 225 elements (viscous case).

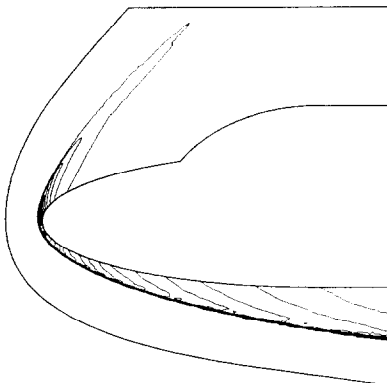


Fig. 4. Pressure contours (inviscid case).

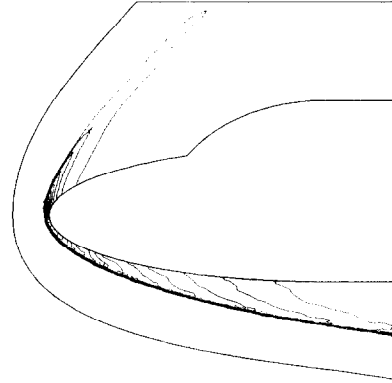


Fig. 5. Pressure contours (viscous case).

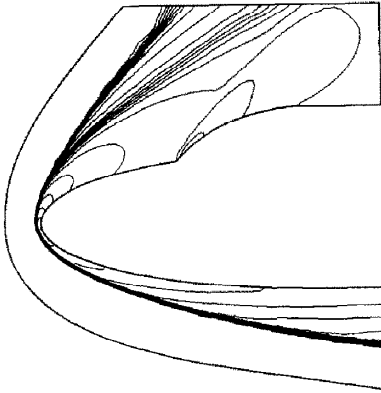


Fig. 6. Temperature contours (inviscid case).

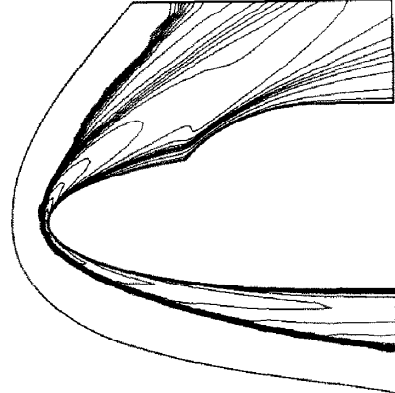


Fig. 7. Temperature contours (viscous case).

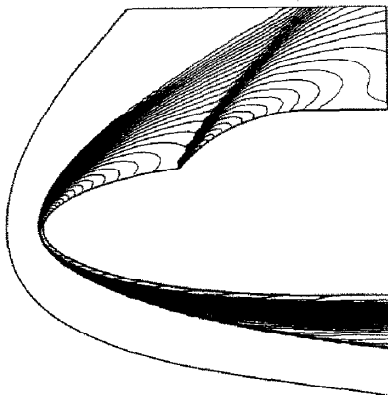


Fig. 8. Atomic nitrogen mass fraction contours (inviscid case).

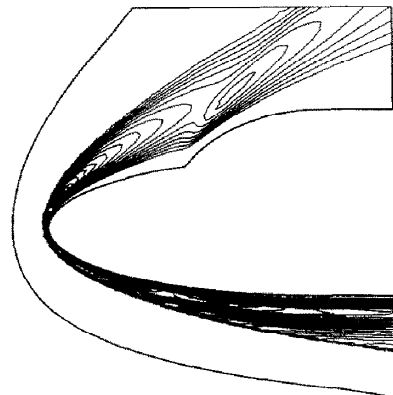


Fig. 9. Atomic nitrogen mass fraction contours (viscous case).

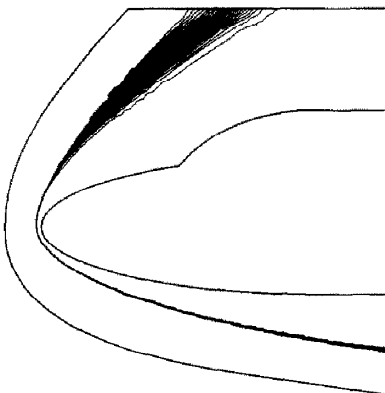


Fig. 10. Atomic oxygen mass fraction contours (inviscid case).

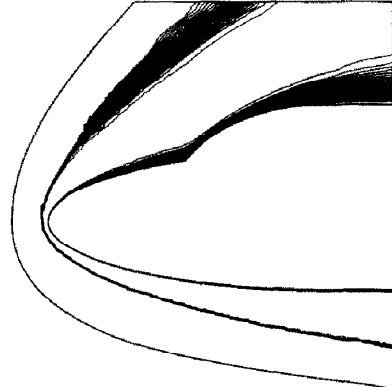


Fig. 11. Atomic oxygen mass fraction contours (viscous case).

6. Conclusion

Consistency has been the leitmotiv of this work, and was indeed one of the main concerns in designing the method. First, the Galerkin/least-squares finite element method is consistent in that it is a residual method: the solution of the initial problem is a solution of the numerical problem. Then, the discretization of the problem is performed consistently, in the sense that no alternations to the physical model nor any additional approximations are required by the numerical method. Finally, the equilibrium chemistry model is consistent, since it uses only the minimum number of theoretical and experimental constants, and thus eliminates any potentially dangerous redundancy. These ingredients result in a mathematically sound flow solver for chemically reacting flows. Clearly, the quality of the numerical results presented here is a strong indication of the benefits derived from the firm mathematical basis of the formulation.

References

- [1] J.D. Anderson, Jr., *Hypersonic and High Temperature Gas Dynamics* (McGraw-Hill, New York, 1989).
- [2] R.S. Shevell, *Fundamentals of Flight*, 2nd Edition (Prentice Hall, Englewood Cliffs, NJ, 1989).
- [3] B. Sweetman, *High Speed Flight* (Jane's, London, 1983).
- [4] United States Committee on Extension to the Standard Atmosphere, U.S. Standard Atmosphere Supplements 1966, U.S. Govt. Print. Off., Washington, 1967.
- [5] W.G. Vincenti and C.H. Kruger, Jr., *Introduction to Physical Gas Dynamics* (Krieger, 1965).
- [6] F. Chalot, T.J.R. Hughes and F. Shakib, Symmetrization of conservation laws with entropy for high-temperature hypersonic computations, *Comput. Systems Engrg.* 1 (1990) 465–521.
- [7] T.J.R. Hughes, Recent progress in the development and understanding of SUPG methods with special reference to the compressible Euler and Navier–Stokes equations, *Internat. J. Numer. Methods Fluids* 7 (1987) 1261–1275.
- [8] T.J.R. Hughes and G.M. Hulbert, Space-time finite element methods for elastodynamics: Formulations and error estimates, *Comput. Methods Appl. Mech. Engrg.* 66 (1988) 339–363.
- [9] T.J.R. Hughes, L.P. Franca and G.M. Hulbert, A new finite element method for computational fluid dynamics: VIII. The Galerkin/least-squares method for advective-diffusive equations, *Comput. Methods Appl. Mech. Engrg.* 73 (1989) 173–189.
- [10] C. Johnson and J. Pitkäranta, An analysis of the discontinuous Galerkin method for a scalar hyperbolic equation, Technical Report MAT-A215, Institute of Mathematics, Helsinki University of Technology, Helsinki, Finland, 1984.
- [11] C. Johnson, U. Nävert and J. Pitkäranta, Finite element methods for linear hyperbolic problems, *Comput. Methods Appl. Mech. Engrg.* 45 (1984) 285–312.
- [12] P. Lesaint and P.-A. Raviart, On a finite element method for solving the neutron transport equation, in: C. de Boor, ed., *Mathematical Aspects of Finite Elements in Partial Differential Equations* (Academic Press, New York, 1974) 89–123.
- [13] T.J.R. Hughes and M. Mallet, A new finite element method for computational fluid dynamics: III. The generalized streamline operator for multidimensional advective-diffusive systems, *Comput. Methods Appl. Mech. Engrg.* 58 (1986) 305–328.
- [14] F. Shakib, T.J.R. Hughes and Z. Johan, A new finite element method for computational fluid dynamics: X. The compressible Euler and Navier–Stokes equations, *Comput. Methods Appl. Mech. Engrg.* 89 (1991) 141–219.
- [15] T.J.R. Hughes and M. Mallet, A new finite element method for computational fluid dynamics: IV. A discontinuity-capturing operator for multidimensional advective-diffusive systems, *Comput. Methods Appl. Mech. Engrg.* 58 (1986) 329–336.
- [16] M. Mallet, A finite element method for computational fluid dynamics, Ph.D. Thesis, Division of Applied Mechanics, Stanford University, 1985.
- [17] M.W. Chase, Jr., C.A. Davies, J.R. Downey, Jr., D.J. Frurip, R.A. McDonald and A.N. Syverud, JANAF thermochemical tables, third edition, *J. Phys. Chem. Ref. Data* 14 (Suppl. 1) (1985).
- [18] Z. Johan, T.J.R. Hughes and F. Shakib, A globally convergent matrix-free algorithm for implicit time-marching schemes arising in finite element analysis in fluids, *Comput. Methods Appl. Mech. Engrg.* 87 (1991) 281–304.
- [19] F. Shakib, T.J.R. Hughes and Z. Johan, A multi-element group preconditioned GMRES algorithm for nonsymmetric systems arising in finite element analysis, *Comput. Methods Appl. Mech. Engrg.* 75 (1989) 415–456.
- [20] J.-A. Désidéri, N. Glinsky and E. Hettner, Hypersonic reactive flow computations, *Comput. & Fluids* 18 (1990) 151–182.